SPECTRALLY-CONSISTENT RELATIVE RADIOMETRIC NORMALIZATION FOR MULTI-TEMPORAL LANDSAT 8 IMAGES

Muhammad Aldila Syariz[1], Chao-Hung Lin[1], and Bo-Yi Lin[1]
[1]Department of Geomatics, National Cheng Kung University, Tainan 701, Taiwan
Email: aldilasyariz@gmail.com, linhung@mail.ncku.edu.tw, pikadp2004@hotmail.com

KEYWORDS: Spectral consistency, relative normalization, pseudo-invariant features (PIFs), multivariate alteration detection, constrained regression

ABSTRACT: Radiometric normalization is a necessary pre-processing step since the acquired satellite images contain uncertainties such as atmospheric effect and surface reflectance. For most historical experiments, the associated atmospheric properties may be difficult to obtain even for planned acquisitions. Relative normalization is an alternative method whenever absolute reflectance properties are not required. The key to relative normalization is the selection of pseudo-invariant features (PIFs) in an image. PIFs of a bi-temporal image is a group of pixels which are statistically nearly-constant over the period of the bi-temporal image acquisitions. Several methods, such as manual selection, histogram matching, and principal component analysis, had been proposed for PIFs extraction. Yet, a change in pixel's spectral signature before and after normalization, called spectral inconsistency, is detected whenever those PIFs extraction methods, associated with a regression process, are performed. To overcome this shortcoming, the commonly used PIFs selection, called multivariate alteration detection (MAD), is utilized as it considers the relationship among bands. Further, a constrained regression is adopted to enforce the normalized pixel's spectral signature to be consistent as possible. This approach is applied to multi-temporal Landsat-8 imageries. Moreover, spectral distance and similarities are utilized for evaluating the consistency of the normalized pixel's spectral signature.

1. INTRODUCTION

Satellite images acquired from the same terrain at different times contain valuable information for regular monitoring of the earth's surface, allowing us to describe the land-cover change, vegetation health, natural hazard events, etc (Lu et al., 2004; Coppin et al., 2004). However, those images often contain some uncertainties due to changes in satellite sensor calibration, differences in illumination and observation angles, variation in atmospheric effects, and changes in target reflectance (Du et al, 2002).

Images normalization is necessary to do as true changes in the image between two acquisition dates are difficult to interpret. Two techniques, absolute and relative, have been developed to correct the acquired images for preserving radiometric accuracy.

The absolute technique aims to transform the digital number into bottom-of-atmosphere reflectance. To do so, this technique relates the digital numbers in satellite image data to reflectance at the surface of the landscape. It requires sensor calibration coefficients, an atmospheric correction algorithm, and related input data, (Du et al., 2002). Fraser et al. (1989), Kaufman (1988), and Kneizys et al. (1983) have resulted in a number of atmospheric correction algorithm that can provide a realistic estimation of the scattering and absorption on the satellite image. However, it is difficult to apply the algorithm due to the minimum knowledge of atmospheric properties. For most historical experiences, the atmospheric properties are difficult to acquire and even are not available (Due et al., 2002).

A relative technique based on the radiometric information is an alternative whenever absolute surface reflectance properties are not required (Canty et al., 2003). This technique aims to put all the images on a common radiometric level (Du et al., 2002). Many methods have been proposed for the relative radiometric normalization of multispectral images taken under different atmospheric conditions at different times. In common, those methods contain two associated statistical steps. They are to select pseudo-invariant features (PIFs) and to extract regression coefficients, respectively.

PIFs is a group of pixels in which their digital numbers are statistically suffering small change over two different image acquisition dates of the same terrain. A number of methods have been proposed for PIFs. All proceed under the assumption that the relationship between the at-sensor reflectance properties recorded at two different times from regions of constant reflectance is spatially homogeneous and can be approximated by linear regression (Du et al., 2002).

Hall et al. (1991) and Schott et al. (1988) are manually inspecting PIFs. This method normalizes images of the same areas through the landscape elements whose reflectance is not changed over time. Caselles and Garcia (1989), Conel

(1990), Coppin and Bauer (1994) have used similar procedures. However, the results might be not reliable since they are subjective to the capability of one who was selecting PIFs.

Du et al. (2002) utilized principal component analysis (PCA) to select PIFs. This technique addresses major and minor axis of a principal component. The pixels around the major axis are considered as PIFs. Further, Lin et al. (2015) insert iterative weighting scheme to PCA for obtaining a more robust set of IPs. However, each band is processed independently in this technique.

Nielsen et al. (1998) and Canty et al. (2004) proposed the use of multivariate alteration detection (MAD) to extract PIFs of bi-temporal images. This technique is invariant to linear and affine scaling. The procedure is simple, fast, and completely automatic and compares very favorably with normalization using hand-selected, time-invariant features. However, Nielsen (2008) and Zhang et al. (2004) found that the existence of changed pixels may affect uncertainties since these pixels are inserted in the calculation of mean and covariance matrix. Hence, an iterative-reweighted strategy is utilized in order to defeat this challenge (Nielsen, 2007; Canty et al., 2008).

Whenever PIFs has been selected, one should further extract linear regression coefficients for putting all the images on a common radiometric scale. Du et al. (2002) utilized ordinary least squares regression (OLS) technique, proposed by Yang and Lo (2000), with quality control to extract linear regression coefficients. With a larger than 0.900 of linear correlation coefficients, the OLS performs well. However, this technique allows for measurement uncertainty (error) in one image only. In case of radiometric normalization, one should assume that the measurement uncertainty is involved in all images. Therefore, Canty et al. (2004) investigated orthogonal regression to perform actual normalization, as it treats the data symmetrically. Since it processes each band independently, this may further cause a shortcoming called spectral inconsistency.

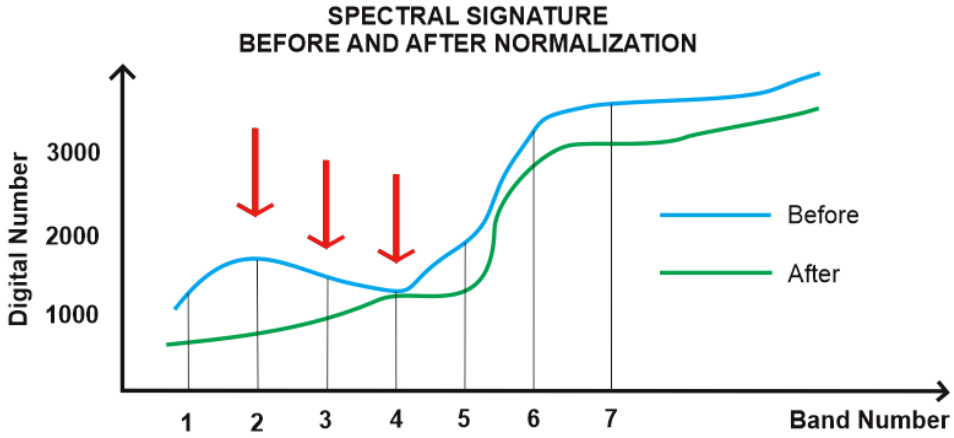

Figure 1. Spectral inconsistency of a pixel's spectral signature before and after normalization

Spectral inconsistency is an inconsistency problem occurred on spectral signature after the image is normalized, as shown in Figure 1. Blue and green lines are the spectral signatures of before and after normalization of the images, respectively. Red arrows indicate the occurrence of spectral inconsistency. Before normalization, the spectral signature of band number 2-4 shows a going down pattern. However, the opposite pattern occurs after the image is normalized.

2. METHODOLOGY

2.1 PIFs Selection using Iteratively-reweighted MAD (IR-MAD)

Suppose we have multi-temporal images, *X* and *Y* which have *p* number of bands and *n* number of pixels. To make a linear combination, we assume *a* and *b* are a pair of multiple vectors for band *i* of image *X* and *Y*, respectively. Thus, we will have some matrices shown in Eq. (1).

$$a = \begin{pmatrix} a_1 \\ a_2 \\ \vdots \\ a_p \end{pmatrix} \qquad b = \begin{pmatrix} b_1 \\ b_2 \\ \vdots \\ b_p \end{pmatrix} \qquad U_{1xn} = a_{px1}^T X_{pxn}, V_{1xn} = b_{px1}^T Y_{pxn} \tag{1}$$

Specifically, we seek linear combinations such that $Var(U-V)$ will be maximum subject to constraints $Var(U) = Var(V) = 1$ and $Cov(U,V) > 0$. Note that under these constraints $Var(U-V) = 2(1-\rho)$, where ρ (Eq. (2)) is the correlation of the transformed vector U and V.

$$\rho = Corr(U,V) = \frac{Cov(U,V)}{\sqrt{Var(U)xVar(V)}} = \frac{a^T \sum_{XY} b}{\sqrt{a^T \sum_{XX} a b^T \sum_{YY} b}} \tag{2}$$

By using Lagrange multipliers, this leads to the coupled generalized eigenvalue problems (Eq. (3)).

$$\begin{matrix} \sum_{XY} \sum_{YY}^{-1} \sum_{YX} a = \rho^2 \sum_{XX} a \\ \sum_{YX} \sum_{XX}^{-1} \sum_{XY} b = \rho^2 \sum_{YY} b \end{matrix} \tag{3}$$

Thus, the desired projections $U_{1xn} = a_{px1}^T X_{pxn}$ are given by the eigenvectors $a_1 \dots a_p$ corresponding to the generalized eigenvalues $\rho_1^2 \geq \cdots \geq \rho_p^2$ of $\sum_{XY} \sum_{YY}^{-1} \sum_{YX}$ respect to $\sum_{XX}$. Similarly the desired projections $V_{1xn} = b_{px1}^T Y_{pxn}$ are given by eigenvectors $b_1 \dots b_p$ of $\sum_{YX} \sum_{XX}^{-1} \sum_{XY}$ with respect to $\sum_{YY}$ corresponding to the same eigenvalues. Nielsen et al (1998) refer to the p difference components $MAD_i = U_i - V_i$.

$$nmad = \sum_{i=1}^{p} \left({}^{MAD_i}/_{\sigma_{MADi}} \right)^2 \tag{4}$$

We can select all pixel coordinates which satisfy $nmad < t$, where t is a decision threshold. Under the hypothesis of no-change, the $nmad$ (Eq. (4)) is approximately chi-squared distributed with p degrees of freedom. We chose $t = \mathcal{X}^2_{p,P=0.01}$, where P is the probability of observing that value of t or lower. The pixels thus selected should correspond to truly PIFs. Thus, the overall radiometric differences between the two images can be attributed to linear effects.

The iteratively-reweighted scheme of MAD is further adopted. Different to Nielsen (2007) who sets initial weight equal to 1 for each pixel, we consider to utilize similarity measurement, e.g. spectral angle (Eq. (5)). Spectral angle ranges from 0° to 90° in which smallest value means the spectral signatures of two corresponding pixels are absolutely similar and highest value means the opposite. This aims to strengthen pixel which exhibits smaller change.

$$SA = \cos^{-1} \frac{\sum_{=1}^{p} Y_i Y'_i}{\sqrt{\sum_{i=1}^{p} Y_i^2 \sum_{i=1}^{n} Y'^2_i}} \tag{5}$$

Further, in the iteration process, Nielsen (2007) utilized probability function of chi-squared distribution in determining the weight's value of each pixel. We further take another different weighting strategy in this following step. Eq. (6) implies the weighting strategy in the iteration process of this study. It aims to strengthen pixels with a smaller value of $nmad$.

$$w_j = \frac{\left[\left(\frac{nmad_j - nmad_{min}}{nmad_{max} - nmad_{min}} * 99 \right) + 1 \right]}{100} \tag{6}$$

2.2 Constrained Regression

After obtaining PIFs, orthogonal regression is performed. This aims to find the normalization coefficient, slope α and intercept β. In this step, the number of α and β are equal to the number of bands. Thus, it leads us to have $\alpha = [\alpha_1 \quad \alpha_2 \quad \cdots \quad \alpha_p]$, $\beta = [\beta_1 \quad \beta_2 \quad \cdots \quad \beta_p]$, and their regression qualities $r^2 = [r_1^2 \quad r_2^2 \quad \cdots \quad r_p^2]$, where those are sequenced following this constraint $\alpha_1 > \alpha_2 > \cdots > \alpha_p$.

In the afore condition, each band's regression might result in a good quality. However, as shown in Figure 2, the elements' value of α and β are random. This may lead to the inconsistency problem. A one linear regression approach might be the solution of the inconsistency problem. However, each band's regression might be suffering a bad r^2. Thus, we proposed to combine the advantage of those two approaches. This combination is to maintain the quality of each band's regression while preserving the pixel's consistency.

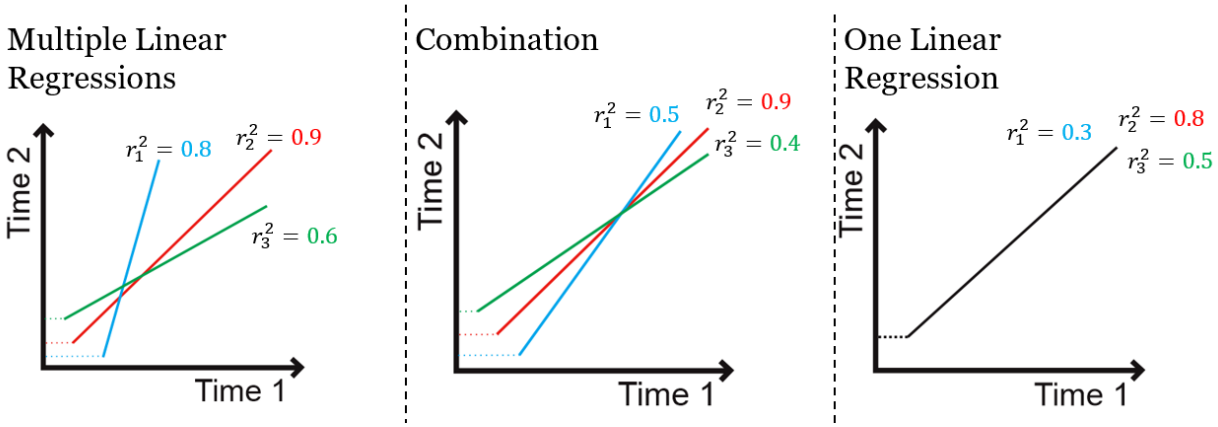

Figure 2. Left: the illustration of linear regression results at time the original approach is conducted; Right: one linear regression approach to defeat the inconsistency problem, yet the qualities of band's regressions are bad; Center: proposed approach which combines the advantage of those two previous approaches

In reaching this goal, we prefer to constrain the regression's coefficients by applying cost function with three weighting schemes. Those weighting schemes aim to preserve the spectral consistency while maintaining the performance of each regression. This further is called as constrained regression.

Several assumptions are provided in this constrained regression process. The assumptions are explained as follows:

1. Each two sequenced elements of α and β should change gradually.
2. Gradients (Eq. (7)) of α and β should be constant.

$$\begin{gathered}\boldsymbol{\nabla\alpha} = [\nabla\alpha_1 \quad \nabla\alpha_2 \quad \cdots \quad \nabla\alpha_{n-1}] = constant \\ \boldsymbol{\nabla\beta} = [\nabla\beta_1 \quad \nabla\beta_2 \quad \cdots \quad \nabla\beta_{n-1}] = constant \\ where\ \boldsymbol{\nabla\alpha_n} = \alpha_{n+1} - \alpha_n\end{gathered} \tag{7}$$

3. Laplacians (Eq. (8)) of α and β should be equal to 0 (zero).

$$\begin{aligned}\boldsymbol{\nabla^2\alpha} &= [\nabla^2\alpha_1 \quad \nabla^2\alpha_2 \quad \cdots \quad \nabla^2\alpha_{n-2}] = 0 \\ \boldsymbol{\nabla^2\beta} &= [\nabla^2\beta_1 \quad \nabla^2\beta_2 \quad \cdots \quad \nabla^2\beta_{n-2}] = 0\end{aligned} \tag{8}$$

The first weighting scheme utilizes the Laplacian form and purposes to fix the inconsistency problem as well as to maintain the initial values of α and β not to change a lot. As shown in Eq. (9), the ω can be adjusted following which purpose we need to prioritize. The illustration of the first weighting scheme is shown in Figure 3.

$$F_1 = \omega[\alpha + \beta] + (1 - \omega)[\nabla^2\alpha + \nabla^2\beta] \tag{9}$$

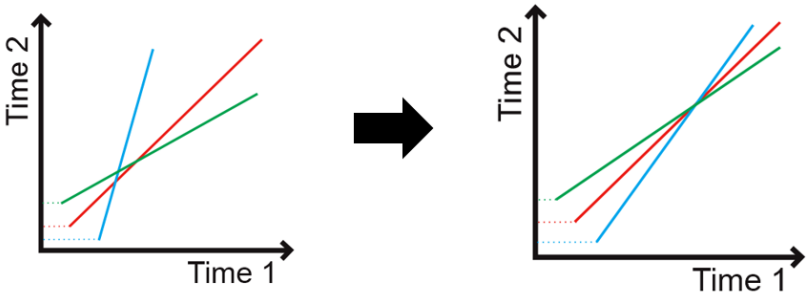

Figure 3. The illustration of the first weighting scheme result

The second weighting scheme utilizes the coefficient of determination of each band. This scheme aims to distribute the uncertainties into all bands on a considerable degree. The band which has a higher coefficient of determination will be distributed less uncertainty, and vice versa (see Eq. (10)). The illustration of second weighting scheme is shown in figure 4.

$$F_2 = \varphi[\alpha + \beta]; where\ \varphi_i = \frac{\left[\left(\frac{r_i^2 - r_{min}^2}{r_{max}^2 - r_{min}^2} * 99\right) + 1\right]}{100} \quad (10)$$

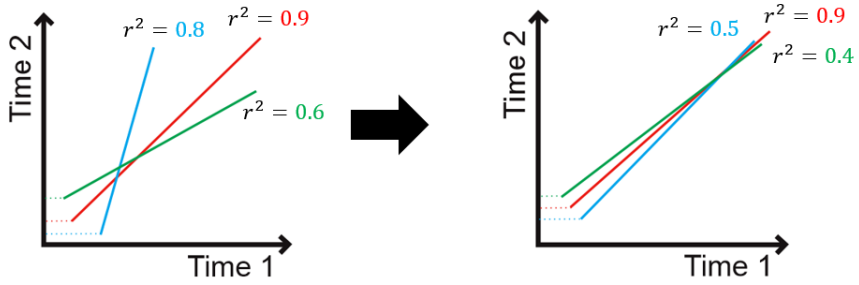

Figure 4. The illustration of the second weighting scheme result

Further, the third weighting scheme utilizes the bands which are involved in the indexing strategy. This scheme aims to distribute fewer uncertainties to the involved bands and more uncertainties to the uninvolved bands. Besides, it prioritizes the involved band(s) not to suffer a high decreasing of r^2 (see Eq. (11)). This weighting scheme is illustrated on Figure 5.

$$F_3 = \kappa[\alpha + \beta]; where\ \kappa_i = \begin{cases} \kappa, & band_n = included \\ 1 - \kappa, & band_n \neq included \end{cases} \quad (11)$$

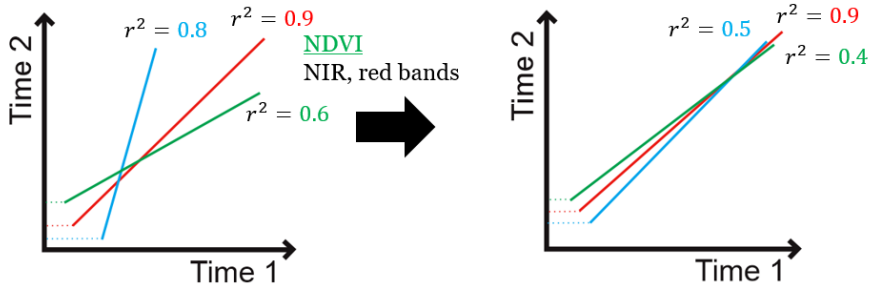

Figure 5. The illustration of the third weighting scheme result

Those weighting schemes will be processed under the iterative scheme as shown in Figure xx. The iteration stops when the value of each element of $\nabla^2\alpha$ and $\nabla^2\beta$ is close to zero.

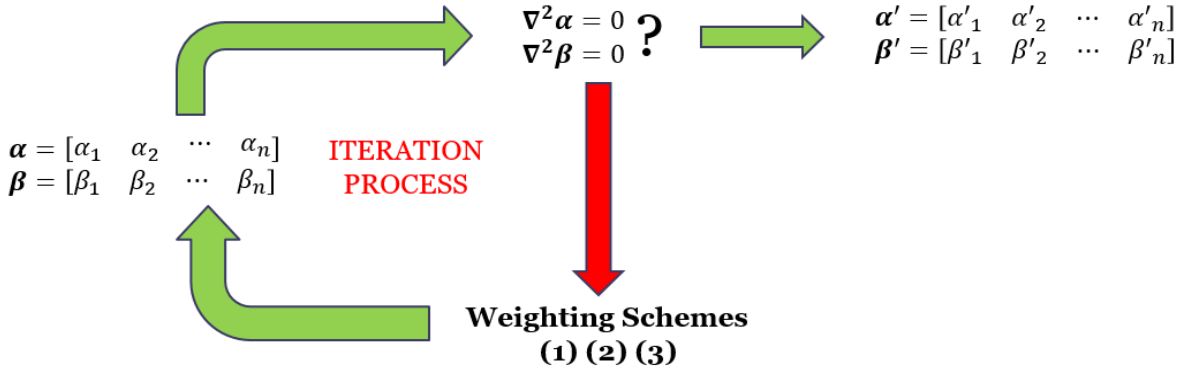

Figure 6. Iterative-weighting process of proposed approach

Hence, distance and similarity measurements are utilized for evaluating the proposed approach. Those measurements are to figure out how far the radiometric level is moving and to find how similar the spectral signature before and after an image is normalized. We adopt Euclidean distance (Eq. (12)) and spectral angle (Eq. (5)), which introduced by Carvalho Junior et al. (2013), to display the evaluation.

$$ED = \sqrt{\sum_{i=1}^{p} (Y_i - Y'_i)^2} \quad (12)$$

3. EXPERIMENTAL RESULTS AND DISCUSSIONS

The spectrally-consistent relative radiometric normalization is performed to bi-temporal Landsat 8 images. Those images are taken in Mexico. One of them is the reference image while other be the target image as shown in figure 7. Several experiments will be conducted by adjusting t, ω, and κ.

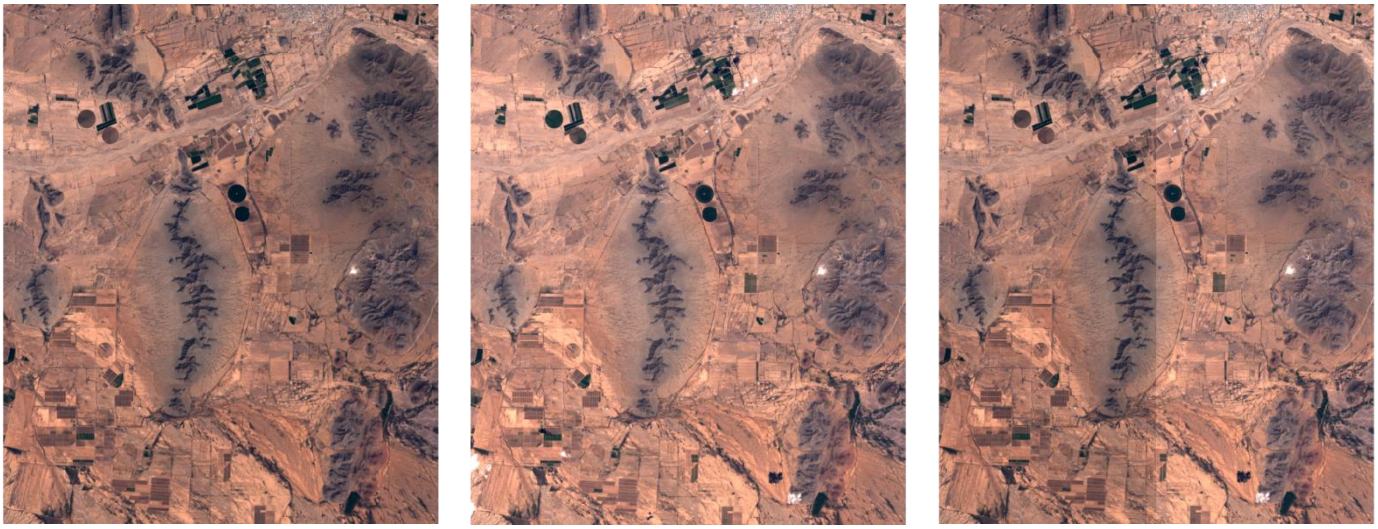

(a) **(b)** **(c)**

Figure 7. (a) Reference image; **(b)** target image; and **(c)** mixture image of reference (left) and target (right)

3.1 Normal Thresholding

In the beginning, we experiment a normal thresholding by adjusting t equals to 4. The PIFs image is shown in figure 8 (a). Black pixels imply the changed pixels while others are PIFs. As shown in table 1, the correlations are more than 0.9500 and it indicates the selection of PIFs is excellent. The α and β are in random condition with r^2 more than 0.9000. Since the *SA* value of this condition is high (3.6589°), the proposed approach need to be implemented.

When implementing the proposed approach, we adjust ω equal to 0.8. It results α and β to be in systematic condition and makes the *SA* value is decreasing. This means the consistency of the spectral signatures becomes better. Yet, it still suffers a worse r^2 than previous. As shown in figure 9 (a) and 9 (b), it is difficult to find differences between those image results. However, those results are statistically different as shown by their *ED* values.

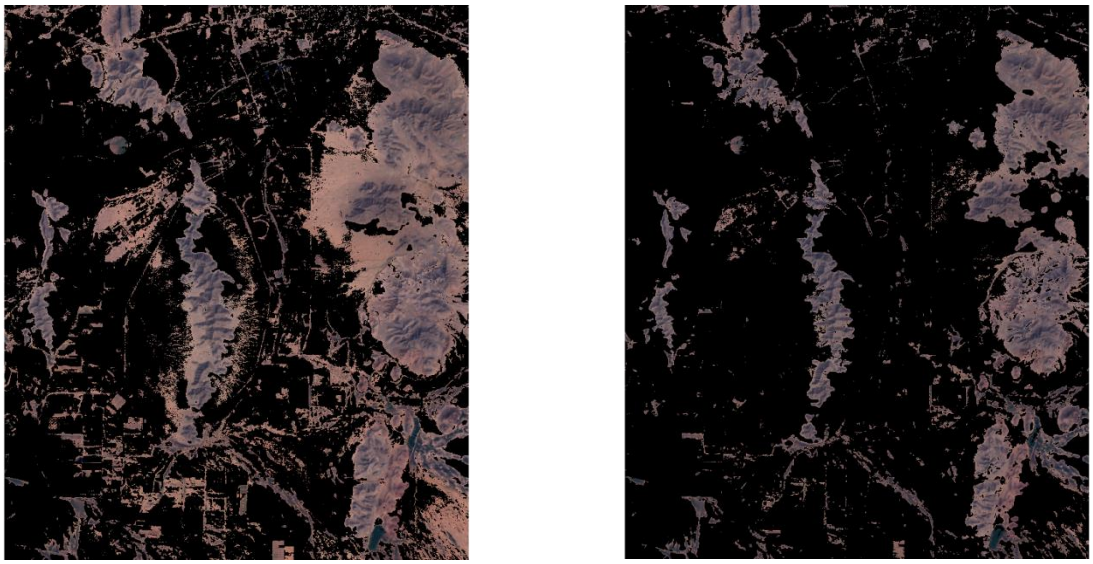

(a) **(b)**

Figure 8. The PIFs selection images of **(a)** normal and **(b)** strict thresholding

Table 1. Statistical experimental results for normal thresholding

t	4											
Experiments	PIFs Quality	Original approach			$\omega = 0.8$ $\kappa = default$			$\omega = 0.2$ $\kappa = default$			$\omega = 0.2$ $\kappa = soil\ index$		
		α	β	r^2	α	β	r^2	α	β	r^2	α	β	r^2
Band 1	0.9698	0.8999	445.9188	0.9393	0.8532	846.5126	0.8213	0.8523	809.9602	0.7386	0.8338	611.6281	-1.0510
Band 2	0.9710	0.9094	288.9864	0.9418	0.8534	846.6143	0.9133	0.8525	810.1852	0.8827	0.8340	612.1021	-0.0030
Band 3	0.9736	0.9329	-40.8806	0.9467	0.8542	847.5153	0.9340	0.8533	812.2874	0.9292	0.8361	618.1425	0.6188
Band 4	0.9719	0.9199	-30.2257	0.9423	0.8535	846.7663	0.9327	0.8526	810.5326	0.9332	0.8344	613.0308	0.8015
Band 5	0.9658	0.9235	-196.8320	0.9307	0.8538	847.1536	0.9178	0.8530	811.4350	0.9141	0.8353	615.6471	0.7674
Band 6	0.9750	0.9412	-484.3847	0.9503	0.8543	847.6377	0.9310	0.8535	812.5771	0.9271	0.8365	619.0450	0.8207
Band 7	0.9742	0.9227	-175.6958	0.9473	0.8537	846.9526	0.9381	0.8528	810.9648	0.9373	0.8348	614.2857	0.8569
Band 8	0.1037	0.2429	3819.9000	-10.5021	0.8532	846.4721	-148.3172	0.8523	809.8818	-66.5246	0.8336	611.5182	-448.0712
Band 10	0.9732	0.9659	2302.4000	0.9481	0.8544	847.7023	-20.9773	0.8536	812.7303	-21.5551	0.8368	619.4392	-29.6850
Band 11	0.9641	0.9279	3293.3000	0.9297	0.8540	847.3480	-28.6432	0.8532	811.8924	-29.4786	0.8357	616.9718	-40.9011
ED	Mean	3229.3219			5129.2000			5256.8000			6622.0000		
SA		3.6589			1.4775			1.4157			1.0743		

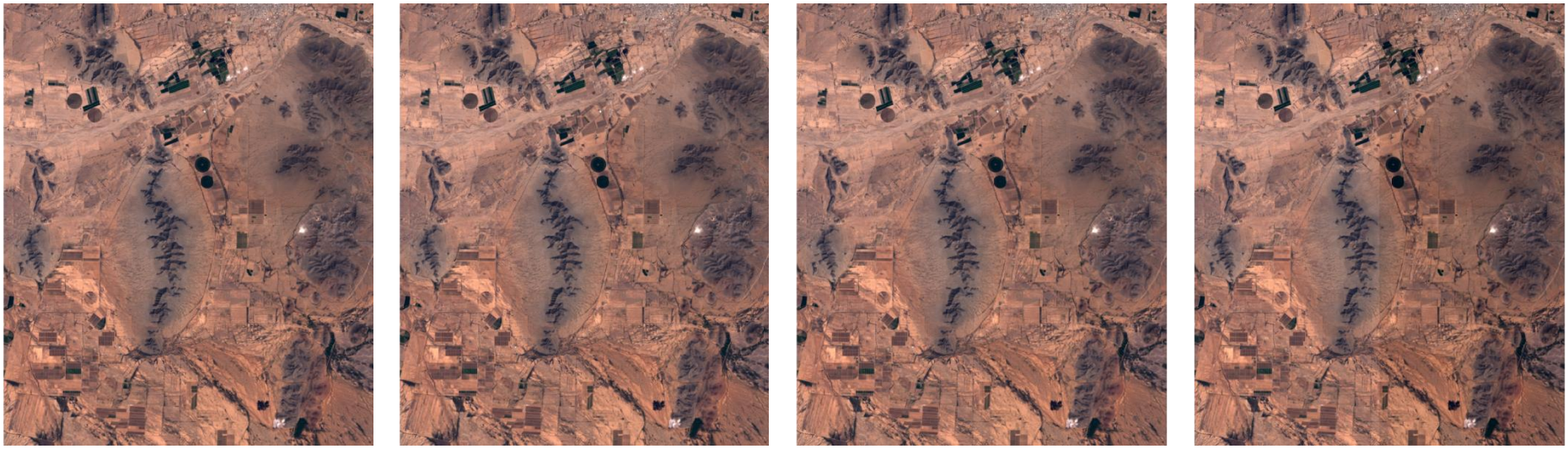

(a) **(b)** **(c)** **(d)**

Figure 9. Normalized images of **(a)** original approach; and proposed approach with **(b)** $\omega = 0.8$, $\kappa = default$; **(c)** $\omega = 0.2$, $\kappa = default$; and **(d)** $\omega = 0.2$, $\kappa = soil\ index$

Table 2. Statistical experimental results for strict thresholding

t	1											
Experiments	PIFs Quality	Original approach			$\omega = 0.2$ $\kappa = default$			$\omega = 0.8$ $\kappa = default$			$\omega = 0.8$ $\kappa = soil\ index$		
		α	β	r^2	α	β	r^2	α	β	r^2	α	β	r^2
Band 1	0.9721	0.9028	404.1797	0.9442	0.8714	551.7454	0.6663	0.8705	577.6717	0.7024	0.8604	459.2344	-0.2104
Band 2	0.9735	0.9169	196.6764	0.9470	0.8715	552.0562	0.8591	0.8706	577.8356	0.8755	0.8605	459.4672	0.4369
Band 3	0.9744	0.9464	-192.8185	0.9487	0.8721	554.4135	0.9288	0.8713	579.0188	0.9320	0.8613	461.4819	0.7799
Band 4	0.9710	0.9333	-197.4064	0.9416	0.8716	552.5359	0.9323	0.8707	578.0807	0.9306	0.8607	459.8680	0.8926
Band 5	0.9650	0.9433	-491.4205	0.9299	0.8719	553.7820	0.9176	0.8711	578.7053	0.9168	0.8611	460.9437	0.8763
Band 6	0.9777	0.9521	-669.8495	0.9552	0.8724	555.3590	0.9429	0.8716	579.4860	0.9422	0.8616	462.3102	0.9181
Band 7	0.9735	0.9373	-389.3681	0.9462	0.8718	553.1327	0.9357	0.8709	578.3812	0.9335	0.8609	460.3861	0.9210
Band 8	0.1271	0.2800	3630.8932	-7.5445	0.8713	551.6371	-64.8367	0.8704	577.6064	-35.1480	0.8603	459.1536	-543.8476
Band 10	0.9735	0.9801	1886.1157	0.9466	0.8725	555.5706	-18.0917	0.8717	579.5903	-18.2470	0.8618	462.4747	-22.2727
Band 11	0.9633	0.9473	2772.1178	0.9259	0.8722	554.9588	-26.4891	0.8714	579.2886	-26.7595	0.8615	461.9527	-32.4912
ED	Mean	3278.9000			4977.2000			4956.3000			5912.5000		
SA		3.6966			0.9528			0.9152			0.7815		

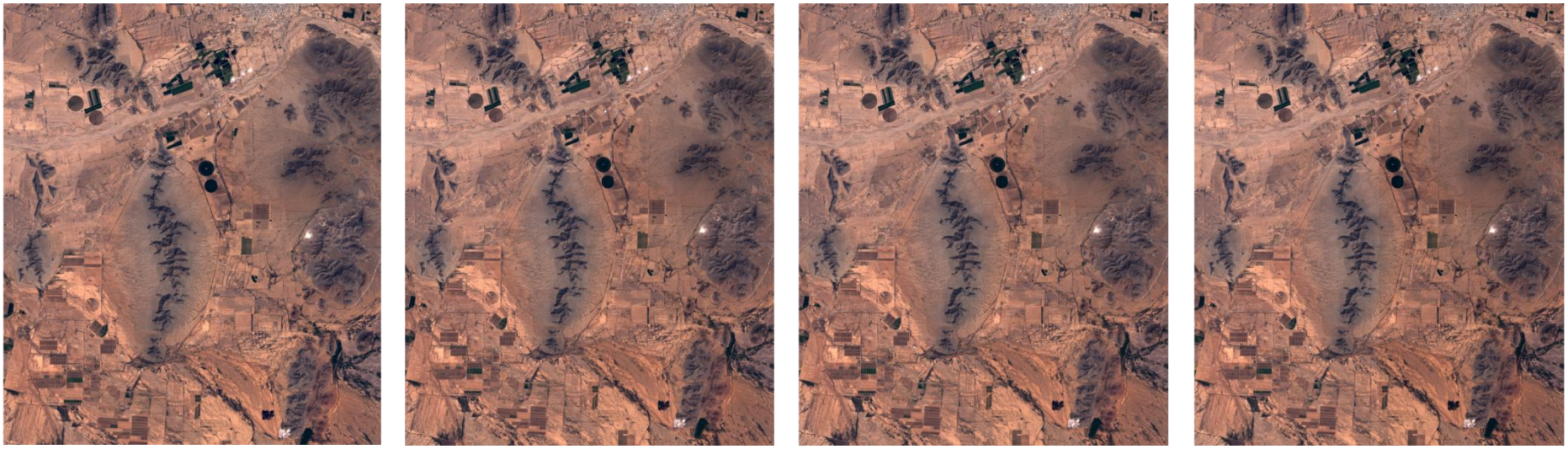

(a) **(b)** **(c)** **(d)**

Figure 10. Normalized images of **(a)** original approach; and proposed approach with **(b)** $\omega = 0.2$, $\kappa = default$; **(c)** $\omega = 0.8$, $\kappa = default$; and **(d)** $\omega = 0.8$, $\kappa = soil\ index$

To maintain the r^2, we further readjust ω to 0.2. This leads to a better r^2. Besides, this also leads to have a better *SA* value. Hence, we adjust κ to soil index. It results a better r^2 and *SA* value. However, the results image suffers difference as it shown in Figure 9. Overall, the experiment with $\omega = 0.2$ and $\kappa = default$ are most suitable for the normal thresholding.

3.2 Strict Thresholding

In this section, we would like to utilize a very good PIFs by utilizing a strict threshold. t is adjusted to 1. Figure 8 (b) shows the PIFs selection result of the strict thresholding. Similar to previous result, black pixels imply the changed pixels and the others are PIFs. Table 2 implies PIFs selection showing a good performance and having a better quality of PIFs selection than normal thresholding.

In the beginning, the original approach is conducted. The α and β are in random condition. Further, we adjust ω to 0.2. It results the r^2 suffering only low change while the *SA* becoming smaller. As shown in Figure 10 (a) and 10 (b), it is difficult to find differences between those image results. However, those results are statistically different as shown by euclidean distance.

We further adjust ω to 0.8. This leads us to have a better result. As shown in table 2, the r^2 changed a few and *SA* is decreasing. Further, when we adjust κ to soil index, the result becomes better. However, it displays that the result image is different to the others since the r^2 becomes worst. Overall, the experiment with $\omega = 0.8$ and $\kappa = default$ fits for the strict thresholding case.

4. CONCLUSION

The spectrally-consistent relative radiometric normalization has been conducted to bi-temporal images of Landsat 8. The results showed this proposed approach can successfully maintain the regression quality while preserving the consistency of a pixels' spectral signature after normalization. The r^2 of our approach is not changed a lot and the *SA* value becomes much better.

REFERENCES

Canty, M. J., Nielsen A. A., and Schmidt M. 2003. *Automatic Radiometric Normalization of Multitemporal Satellite Imagery.* Remote Sensing of Environment 91, 441-451.

Canty, M. J. and Nielsen A. A. 2007. *Automatic Radiometric Normalization of Multitemporal Satellite Imagery with the Iteratively Re-weighted MAD Transformation*. Remote Sensing of Environment 112, 1025-1036.

Carvalho Junior, O. A., Guimaraes, R. F., Silva, N. C., Gillespie, A. R., Trancoso Gomes, R. A., Silva, C. R., and Ferreira de Carvalho, A. P. 2013. *Radiometric Normalization of Temporal Images Combining Automatic Detection of Psudeo-invariant Features from the Distance and Similarity Spectral Measures, Density Scatterplot, and Robust Regression*. Remote Sensing 5, 2763-2794.

Caselles, V., & Lopez Garcia, M. J. 1989. *An Alternative Simple Approach to Estimate Atmospheric Correction in Multitemporal Studies*. International Journal of Remote Sensing 10, 1127 – 1134.

Conel, J. E. 1990. *Determination of Surface Reflectance and Estimates of Atmospheric Optical Depth and Single Scattering Albedo from Landsat Thematic Mapper Data*. International Journal of Remote Sensing, 11, 783 – 828.

Coppin, P., Jonckheere, I., Nackaerts, K., Muys, B., Lambin, E., 2004. Review article digital change detection methods in ecosystem monitoring: a review. International Journal of Remote Sensing 25, 1565–1596.

Coppin, P. R., & Bauer, M. E. 1996. *Digital Change Detection in Forest Ecosystems with Remote Sensing Imagery*. Remote Sensing Reviews 13, 207 – 234.

Du, Y., Teillet P. M., and Cihlar, J. 2002. *Radiometric Normalization of Multitemporal High-resolution Images with Quality Control for Land-cover Change Detection.* Remote Sensing of Environment 82, 123-134.

Hall, F. G., Strebel, D. F., Nickeson, J. E., and Goetz, S. J. 1991. *Radiometric Rectification: Toward a Common Radiometric Response Among Multi-data, Multi-sensor Images*. Remote Sensing of Environment 35, 11-27.

Kaufman, Y. J. 1988. *Atmospheric Effect on Spectral Signature*. IEEE Transaction on Geoscience and Remote Sensing 26, 441-451.

Lin, C. H., Lin B. Y., Lee K. Y., and Chen Y. C. 2015. *Radiometric Normalization and Cloud Detection of Optical Satellite Images using Invariant Pixels.* ISPRS Journal of Photogrammetry and Remote Sensing 106, 107-117.

Lu, D., Mausel, P., Brondizio, E., and Moran, E. 2004. *Change Detection Techniques*. International Journal of Remote Sensing, vol. 25, no. 12, 2365-2407.

Moran, M. S., Jackson R. D., Slater P. N., and Teillet P. M. 1992. *Evaluation of Simplified Procedures for Retrieval of Land Surface Reflectance Factors from Satellite Sensor Output.* Remote Sensing of Environment 41, 160-184.

Nielsen, A. A., Conradsen, K., and Simpson, J. J. 1998. *Multivariate Alteration Detection (MAD) and MAF Postprocessing in Multispectral, Bitemporal Image Data: New Approaches to Change Detection Studies*. Remote Sensing of Environment 64, 1-19.

Nielsen, A. A. 2007. *The Regularized Iteratively Reweighted MAD Method for Change Detection in Multi- and Hyperspectral Data*. IEEE Transactions on Image Processing 16, 463-478.

Schott, J. R., Salvaggio C., and Volchok W. J. 1988. *Radiometric Scenes Normalization using Pseudo-invariant Features.* Remote Sensing of Environment 26, 1-16.

Yang, X., and Lo, C. P. 2000. *Relative Radiometric Normalization Performance for Change Detection From Multi-date Satellite Images*. Photogrammetric Engineering and Remote Sensing 66, 967-980.

Zhang, L., Liao, M., Wang, Y., Lu, L., and Wang, Y. 2004. *Robust Approach to the MAD Change Detection Method*. Proceedings of SPIE 5574, 184-193.